THE JOURNAL OF PHYSICAL CHEMISTRY Letters

Letter

pubs.acs.org/JPCL

Antibody Subclass Detection Using Graphene Nanopores

Amir Barati Farimani, Mohammad Heiranian, Kyoungmin Min, and Narayana R. Aluru*

Department of Mechanical Science and Engineering, Beckman Institute for Advanced Science and Technology, University of Illinois at Urbana−Champaign, Urbana, Illinois 61801, United States

Supporting Information

ABSTRACT: Solid-state nanopores are promising for label-free protein detection. The large thickness, ranging from several tens of nanometers to micrometers and larger, of solid-state nanopores prohibits atomic-scale scanning or interrogation of proteins. Here, a single-atom thick graphene nanopore is shown to be highly capable of sensing and discriminating between different subclasses of IgG antibodies despite their minor and subtle variation in atomic structure. Extensive molecular dynamics (MD) simulations, rigorous statistical analysis with a total aggregate simulation time of 2.7 μs, supervised machine learning (ML), and classification techniques are employed to distinguish IgG2 from IgG3. The water flux and ionic current during IgG translocation reveal distinct clusters for IgG subclasses facilitating an additional recognition mechanism. In addition, the histogram of ionic current for each segment of IgG can provide high-resolution spatial detection. Our results show that nanoporous graphene can be used to detect and distinguish antibody subclasses with good accuracy.

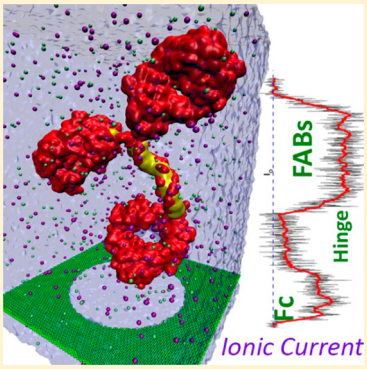

Despite significant advances in the detection, separation, and counting of single proteins with solid-state nanopores,[1−5] atomically resolved scanning of the protein structure remains a significant challenge. In most nanopore-based DNA sequencing[6−11] and single-molecule detection techniques,[12] ionic current blockade and blockade duration are the primary signatures associated with reading and scanning.[6,13−15] Although these techniques are good enough for single-molecule detection, they are not sophisticated enough to analyze and detect fine structures, homologues, and mutagenesis.[12] For example, many subtle differences in antibody proteins, specifically in Immunoglobin Gamma (IgG) subclasses, lie in the number of amino acid compositions and disulfide bonds in their hinge region. Reading and discriminating between these minute structural differences require high-resolution, single-atom thick nanopore technology. In addition to the thickness of the nanopore, the ionic current blockade profile and the chemistry of the nanopore are significant factors in defining the resolution of the nanopore sensor. Biological nanopores[16,17] are too small (~2 nm diameter pore) to study large molecules such as natively folded proteins and antibodies.[10,18,19] To-date, all fabricated solid-state nanopores are so thick (e.g., the Si_3N_4 functionalized pore has a thickness of 5−10 nm) that they completely envelope the whole protein.[2,20] As a result, the ionic current read by the nanopore sensor represents the single protein as a whole.[3,13] The thickness of these membranes highly limits the potential to scan the spatial biological degeneracies and structure of the proteins at the single-atom level.[10,12,19,21−23]

Graphene is a robust, single-atom thick lattice of carbon atoms with high electrical conductivity[24] and mechanical strength. The attractive properties of graphene can be exploited for high-resolution, nanopore-based sequencing of single DNA molecules.[10,25−28] The small thickness (0.34 nm) of the graphene membrane combined with the chemical inertness[25] provides good spatial resolution/reading of the nucleic acid.[27,29,30] Graphene nanopores can also be easily configured,[28,31] resized,[32,33] and anchored with biological markers.[23,34] The single-atom thick graphene nanopore can read the DNA bases at atomic scale by taking advantage of the ionic current blockade.[35] Prior research has shown that graphene can also be used to detect DNA bases in the transverse direction by using quantum tunneling currents.[36] Quantum conductance tunneling in the transverse direction of graphene can detect the bases with good resolution.[37−39]

In this study, we investigate graphene nanopores for scanning and detection of protein structures. Specifically, we focus on the detection of IgG subclasses. Detection, counting, and distinguishing IgG subclasses is of utmost importance in immunocompetitive processes and immunology.[40] In fact, statistics of IgG subclasses in human serum are important toward mapping the immune system of the body and the attributed diseases. Perhaps, as a general concept, the proteome is a better molecular signature of the health status of humans than the genome; however, proteomic data are much more difficult to acquire and analyze.[37]

In this work, we investigate different signals (Figure 1a) for discrimination of IgG subclasses. By computing the ionic current, the dwell time of the ionic current states, and the flux of water molecules through a graphene nanopore for IgG2 and IgG3 subclasses and clustering the ionic current−dwell time and water flux−current data, we demonstrate that IgG

Received: February 16, 2017
Accepted: March 21, 2017
Published: March 21, 2017

DOI: 10.1021/acs.jpclett.7b00385
J. Phys. Chem. Lett. 2017, 8, 1670−1676

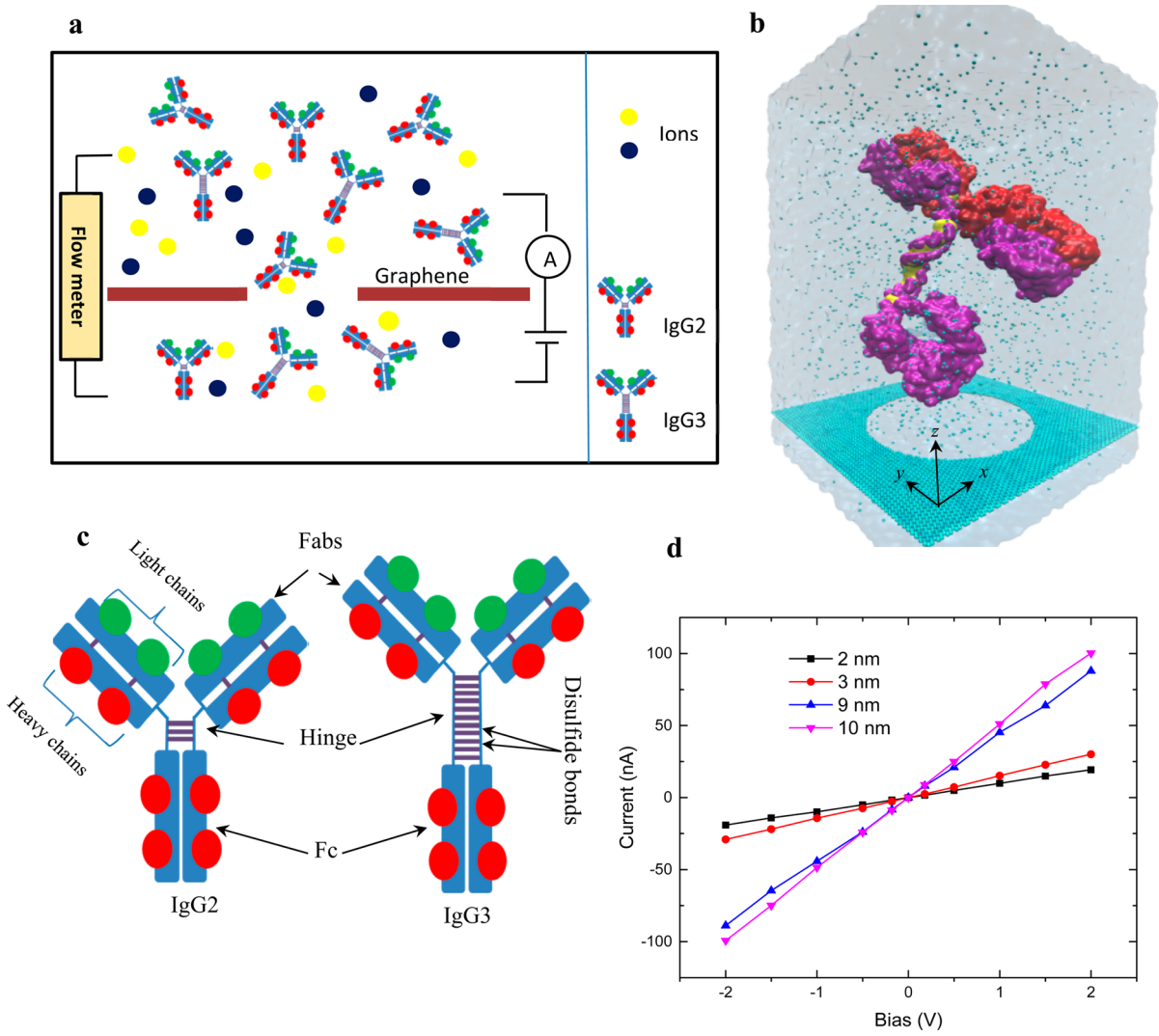

Figure 1. (a) Cartoon representation of a nanoporous graphene protein sensor and scanner. Ions (dark blue and yellow) are electrokinetically driven through the pore by applying an electrical potential gradient. Proteins (here IgG2 and IgG3) are scanned and detected by ionic current and water flux. (b) Simulation system consisting of IgG3 protein (red: light chains; violet: heavy chains; yellow: disulfide bonds in the hinge region), ions (pale green), and graphene (green). (c) Comparison of the structural differences in IgG2 and IgG3. The most notable difference between IgG subclasses is in the hinge regions with variable number of amino acids and disulfide bonds in cysteine residues. (d) Characteristic $I-V$ curves of the graphene nanopores with four different pore sizes.

subclasses are distinguishable. The supervised machine learning (ML) algorithm is used to cluster the sensor data of current–dwell time–water flux.

We performed extensive molecular dynamics (MD) simulations with NAMD 2.6.[41] The visualization of a typical simulation setup consisting of the protein, graphene nanopore, water, and ions (~700 000 atoms) is shown in Figure 1b. IgG, which is a protein complex composed of four peptide chains, contains two identical heavy chains and two identical light chains arranged in a Y-shape (Figure 1c). The four subclasses of IgG show more than 95% homology in the amino acid sequences of the constant domains.[42,43] The four IgG subclasses show their most conspicuous differences in the amino acid composition and structure of the "hinge region", which is part of the molecule containing disulfide bonds (in cysteine residues) between the Y-heavy chains (Figure 1c). For IgG2, we used the intact structure of anticanine lymphoma monoclonal antibody (IgG2a with PDB code: 1IGT).[44] For IgG3, we reconstructed the hinge region (with 11 disulfide bonds) based on the amino acid decomposition described in ref 45 (IgG2 and IgG3 structures are shown in Figure 1c). A pore with a diameter of 10.0 nm was drilled in the center of a 20 nm × 20 nm single-layer graphene. All graphene atoms were fixed in space. Our initial studies show that a pore diameter of less than 10 nm cleaves the IgG proteins. Initially, proteins were placed at the mouth of the graphene nanopore where the protein axis (z direction) is along the graphene pore axis (Figure 1b). Proteins and graphene nanopores were submersed in water and salt ionic solution. The ionic concentration of NaCl was 0.5 M. We used the CHARMM27 force field[46] parameters for all of the proteins, TIP3P water molecules, graphene, and ions. The SHAKE algorithm was used to maintain the rigidity of the water molecules. The periodic boundary condition was applied in all three directions. The cutoff distance for the Lennard–Jones interactions was 15 Å. The long-range electrostatic interactions were computed by using the particle mesh Ewald (PME) method.[47] The time step was selected to be 1 fs. For each simulation, energy

DOI: 10.1021/acs.jpclett.7b00385
J. Phys. Chem. Lett. 2017, 8, 1670–1676

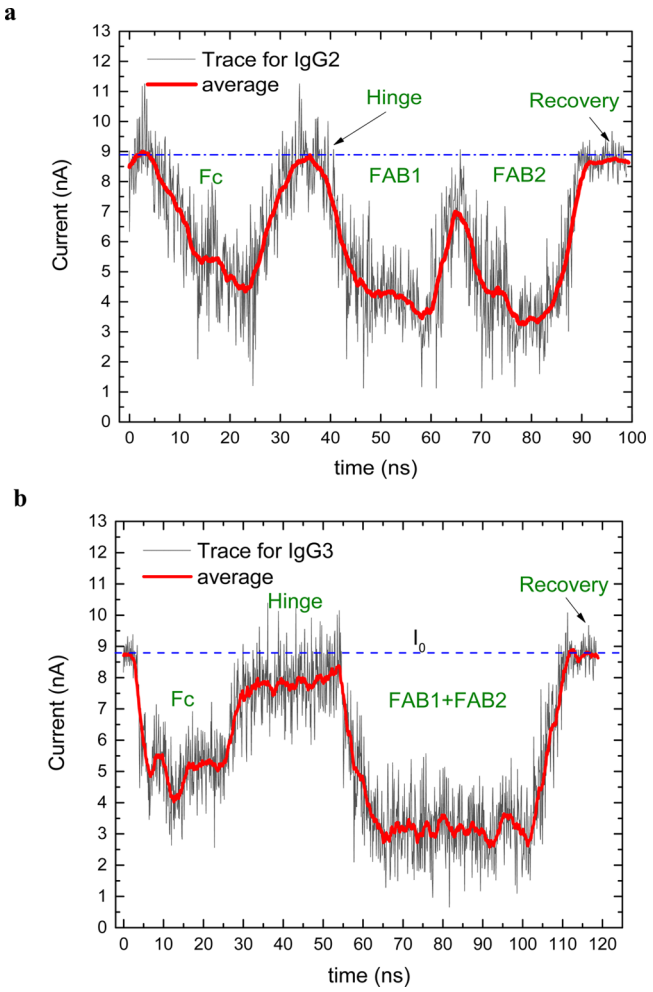

Figure 2. Time-dependent ionic current of (a) IgG2 (b) IgG3 translocation through a pristine 10 nm diameter graphene nanopore. The blue dashed line represents I_0 (graphene nanopore ionic current for the same applied bias (V = 180 mV) without protein translocation). The trace and moving averaged ionic currents are presented in black and red, respectively.

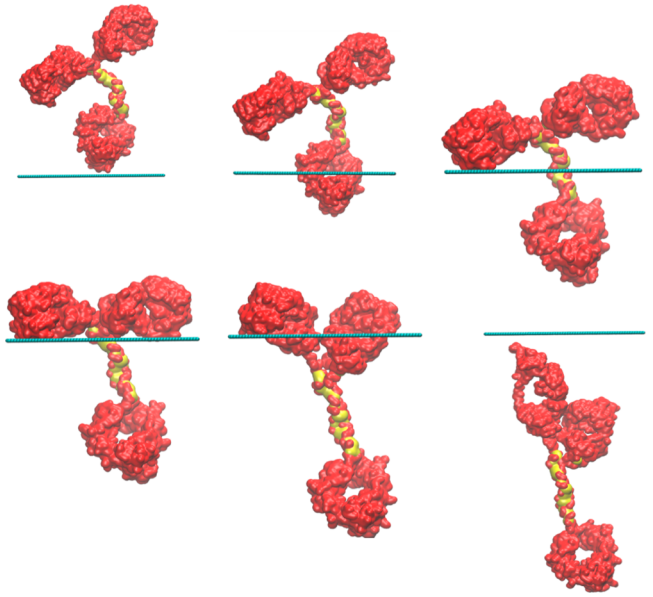

Figure 3. Snapshots of conformational changes and translocation history of IgG3 through a graphene nanopore (yellow color in the hinge region represents the disulfide bonds); similar snapshots for IgG2 are presented in the Supporting Information.

minimization was performed for 100 000 steps. Systems were then equilibrated for 1 ns in an *NPT* ensemble at 1 atm pressure and 300 K temperature. *NPT* simulation ensures that the water concentration is equal to the bulk value of 1 g/cm^3. The simulation was then performed in the *NVT* ensemble. The temperature was maintained at 300 K by applying the Nosè-Hoover thermostat with a time constant of 0.1 ps. Before applying the electric field, equilibration for 2 ns was performed in *NVT*. Production simulations were performed by applying an external electric field in the z direction. The external electric fields are reported in terms of a transmembrane voltage difference $V = EL_z$, where E is the electric field strength and L_z is the length of the simulation system in the z direction.[33] To overcome computational limitations and gather more statistical sampling, we applied two different uniform gravity fields on the antibody molecules, resulting in an accelerated translocation time. For the long time simulations (~100 ns), a gravity of 0.0039 nm/ps^2 was applied, whereas stronger gravities of 0.0293 ± 0.005 nm/ps^2 (resulting in ~25 ns long simulations) were applied to collect enough statistics and construct the signal histograms. For each subclass, we ran 50 simulations (in total 100 simulations for IgG2 and IgG3, for 25 ns each, resulting in an aggregate simulation time of 2.5 μs) with different initial orientations of IgG to account for different possible translocations in experiments (see the Supporting Information for the orientations used). We monitored the time-dependent ionic current, $I(t)$, in the pore. We computed the ionic current through the nanopore by using the definition of current, $I = \mathrm{d}q/\mathrm{d}t$, as $I(t) = \frac{1}{L_z}\sum_{i=1}^{n} q_i\left[\frac{z_i(t+\delta t) - z_i(t)}{\delta t}\right]$, where the sum is for all of the ions, δt is chosen to be 5 ps, z_i and q_i are the z coordinate and charge of ion i, and n is the total number of ions, respectively. The dwell time is simply the duration of a specific current level due to the translocation of a molecule through the nanopore. We computed the time-dependent flux of water through the graphene nanopore by counting the net amount of water molecules transported through the pore every 0.25 ns.[48] The supervised ML (k-means algorithm)[49] used in clustering analysis was performed using Origin (OriginLab, Northampton, MA) software. In the k-means algorithm, a set of n observations (x_1, x_2, ..., x_j, ..., x_n) are assigned to a set of k clusters (c_1, c_2, ..., c_i, ..., c_k) such that the within-cluster sum of squares $\sum_{i=1}^{k}\sum_{\substack{j=1\\ x_j\in c_i}}^{n} \|x_j - \overline{c}_i\|^2$ is minimized, where $\overline{c}_i$ is the center of the ith cluster.

The I–V curves for different size nanopores in graphene, in the absence of the protein, show an Ohmic behavior (Figure 1d). The conductance (G) is computed to be 9.91, 15.2, 45.3, and 51.11 nS for the 2, 3, 9, and 10 nm diameter pores, respectively. These conductance values are comparable to the experimental conductance values (conductance of ~55 nS for 8 ± 1 nm pores) for graphene nanopores of similar sizes.[25] In addition, the conductance values from the simulations are in good agreement with the values predicted by the model developed by Wananu et al.[50] (see the Supporting Information).

We performed two very slow translocations of IgG2 and IgG3 to observe the ionic current trace as a function of time.

DOI: 10.1021/acs.jpclett.7b00385
J. Phys. Chem. Lett. 2017, 8, 1670–1676

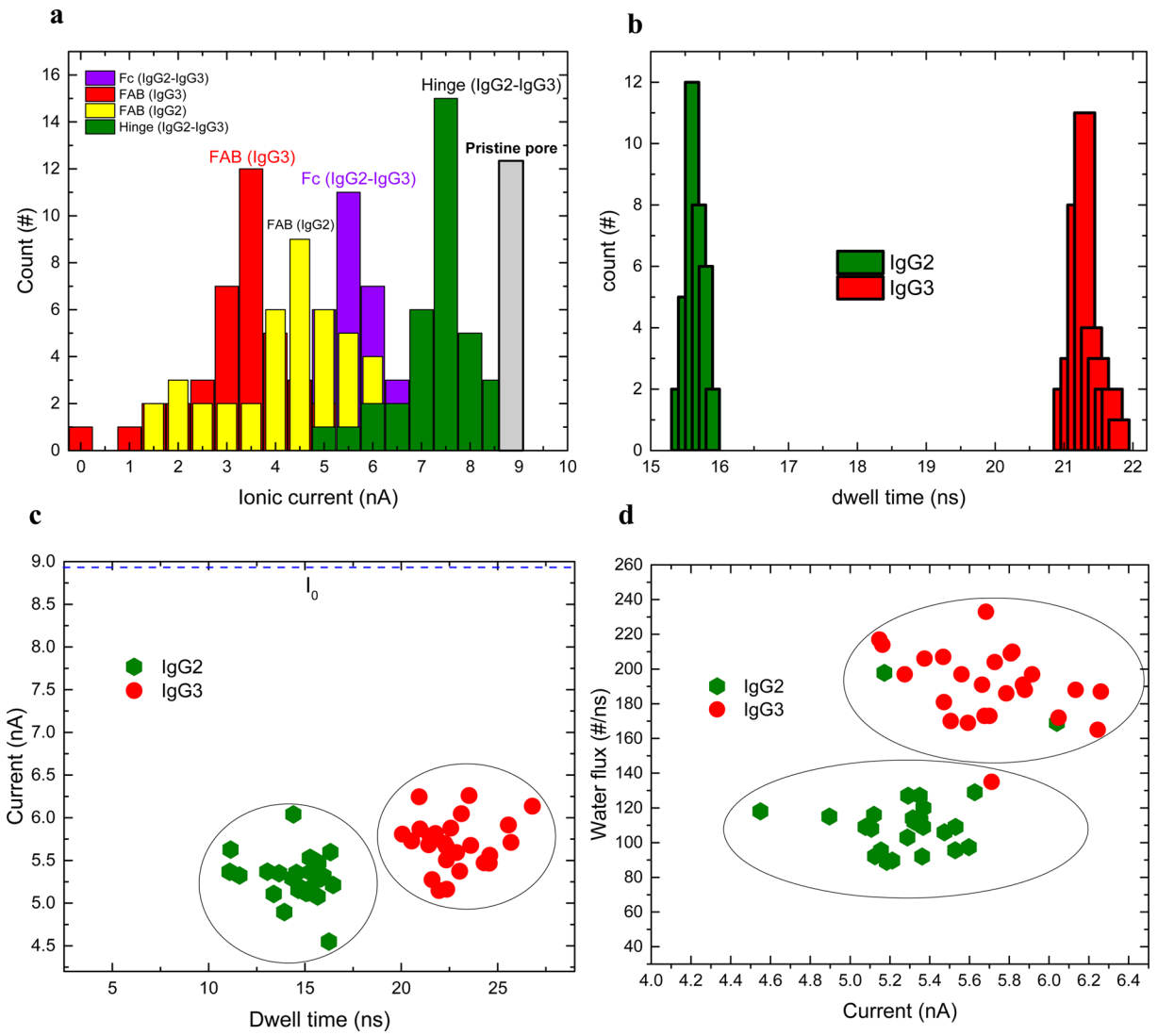

Figure 4. (a) Ionic current histogram of FAB IgG2, FAB IgG3, FC (both IgG2 and IgG3), the hinge region (both IgG2 and IgG3), and a pristine graphene pore. The width of the bars is 0.5 nA, and the height of the bars denotes the number of times an ionic current range has been observed. (b) Histogram of dwell times of IgG2 and IgG3 antibody proteins. The width of the bars is 0.1 ns, and the height of the bars denotes the number of times a dwell time range has been observed. (c) Clustering of ionic current versus dwell time data for IgG2 and IgG3. (d) Clustering of water flux versus ionic current data for IgG2 and IgG3.

The slow translocations mimic the experimental conditions to the extent possible, and they also provide better statistics. The complete translocation of IgG2 and IgG3 through the graphene nanopore took 91 and 111 ns, respectively (Figure 2a,b). The current traces reveal distinguishable features, such as the dwell time corresponding to the length of the hinge region, during the translocation of IgG2 and IgG3 through the 10 nm diameter graphene nanopore (Figure 2a,b). The ionic currents are on the order of ∼9 nA, which are consistent with experimental results.[1] In the time-dependent ionic current plots, the molecular features of the protein are reflected in the ionic current fluctuations as the protein translocates through the nanopore. I_0 represents the statistically averaged ionic current for the graphene nanopore, which is 8.82 nA, in the absence of protein, for an applied potential of V = 180 mV (dashed line in Figure 2a,b). As the IgG protein translocates, FC blocks the pore to a large extent (Figure 2a,b). When FC translocates through the pore, the averaged ionic current of FC drops to 4.5−5.5 nA ($0.51I_0$−$0.62I_0$). After FC has translocated, the hinge region crosses the nanopore. A significant current recovery is observed during hinge translocation, with hinge current blockade durations of ∼17 and ∼28 ns for IgG2 and IgG3, respectively. The approximate translocation time for each hinge disulfide bridge is 2.54 ns (computed for the 11-IgG3-cystine translocation). On the basis of our calculations, on average, the hinge region ionic current is $0.93I_0$. The combination of translocation time and ionic current of the hinge region can be used to discriminate between IgG subclasses as the minor structural differences in the subclasses lie within the hinge region and the number of disulfide bonds. Another striking difference between IgG2 and IgG3 ionic current signatures is associated with the FAB current. IgG2 FABs translocate separately, while IgG3 FABs translocate together and simultaneously through the pore. In Figure 3, snapshots of IgG3 translocation and the conformational changes due to its interaction with graphene show the simultaneous translocation of FABs (see the Supporting Information for the comparison of the conformational changes

DOI: 10.1021/acs.jpclett.7b00385
J. Phys. Chem. Lett. 2017, 8, 1670−1676

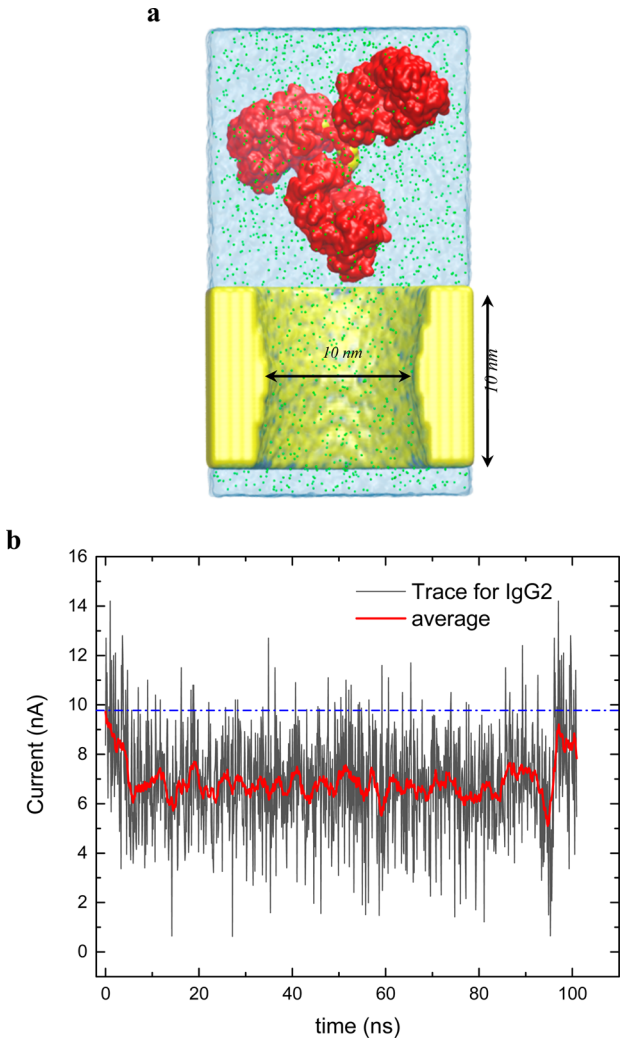

Figure 5. (a) Simulation setup for IgG2 translocation through a Si_3N_4 nanopore. (b) Time-dependent ionic current for IgG2 translocation through a Si_3N_4 solid-state nanopore. The trace and moving averaged ionic currents are shown in black and red, respectively.

of IgG2 and IgG3 during translocation). Figure 2a shows a current recovery between FAB1 and FAB2 translocation for IgG2 (at t = 65 ns), while Figure 2b shows no current recovery for IgG3 FABs translocation.

Figure 2 only presents the signals for one translocation event. More simulations were performed to gather better statistics of the signals for each segment of IgGs. Fifty distinct and complete translocation simulations were carried out for each antibody by considering different orientations (see the Supporting Information for snapshots of the orientations of antibody with respect to graphene) and gravities (0.0293 ± 0.005 nm/ps^2). The histograms of the ionic currents are reported separately for the FAB, FC, and the hinge region (Figure 4a). The histogram is constructed based on the average ionic current of the FC, FAB, and hinge region during the translocation of both antibodies. Because IgG3 FABs translocate together, we reported the ionic current of IgG2 and IgG3 separately. The pristine graphene nanopore ionic current, without any protein, is 8.82 nA for a diameter of 10 nm and bias of 180 mV (the gray bar in Figure 4a). The hinge ionic current histogram has a peak at 7.5 nA with an average of 7.34 nA. The hinge has the highest current among all of the segments of the antibody due to its minimal pore blockage. The FC, FAB (IgG2), and FAB (IgG3) ionic currents have peaks of 5.5, 4.5, and 3.5 nA (with an average of 5.46, 4.51, and 3.57 nA), respectively. The IgG3 FAB has lower ionic current compared to that of IgG2 FAB due to the double FAB blockage of the pore by IgG3.

The dwell time associated with the entire translocation of each antibody is reported for 25 simulations (per antibody subclass; in total 50 simulations) where the gravity is held constant at 0.0293 nm/ps^2 (Figure 4b). The gravity is held constant in all of the simulations to ensure fair comparison of dwell times. The dwell times of IgG3 and IgG2 are clearly different (Figure 4b). The peak to peak dwell time difference is 6 ns (Figure 4b). This gap increases as the applied gravity decreases, which is evident in the total translocation time of the long ∼100 ns trajectories (Figure 2a,b).

The total ionic current (the averaged current for the entire translocation), dwell time, and water flux associated with each translocation are fed into the k-means clustering model. The signals selected for feature extraction are (ionic current, dwell time) and (ionic current, water flux). Fifty data points that are a mixture of both IgG2 and IgG3 averaged features were used. For the ionic current−dwell time feature, the k-means algorithm found two clusters with 100% accuracy (Figure 4c). The data are well clustered into two distinguishable groups with centroid coordinates of (5.29, 14.56) and (5.7, 22.81) for IgG2 and IgG3, respectively. The population of each cluster is 25 data points, which is exactly the number of simulations for IgG2 and IgG3 simulations. In practice, ML analysis becomes important when the dwell times of antibodies overlay each other. In the other clustering, water flux and ionic currents were used as features. The scattered mean cluster plot of the water flux−total ionic current showed relatively distinctive clusters with centroid coordinates of (5.29, 109.22) and (5.7, 191.99) for IgG2 and IgG3, respectively (Figure 4d). In the water flux−ionic current clustering, 2 out of 25 data points of IgG2 were clustered as IgG3 and one IgG2 data point was read as IgG3 by the k-means algorithm (94% accuracy). It should be mentioned that more data will help to train a better model for distinguishing using ML.

To compare the performance of a graphene nanopore with a solid-state nanopore (Si_3N_4),[1,2,21] we translocated IgG2 through a solid-state nanopore (Figure 5a) with a diameter of 10 nm (the same diameter as that of the graphene nanopore) and an applied potential difference of V = 180 mV (see simulation details in the Supporting Information). The length of the solid-state nanopore was 10 nm. Because the architecture of the Si_3N_4 pore is of the converging−diverging conical channel and the constriction regions of the Si_3N_4 and graphene nanopores are similar in diameter (10 nm), the dwell times of both nanopores are expected to be in the same range. In fact, the protein does not experience high frictional resistance in the entrance and exit regions of the Si_3N_4 nanopore. During the translocation of IgG2, the solid-state nanopore envelopes the entire protein, mixing the currents from different fragments of IgGs. We observed a flat, indistinguishable current during translocation of IgG2 (Figure 5b). Thus, many structural details of IgGs are missed with a solid-state nanopore (compare Figure 5b with Figure 2a). Our finding is consistent with the experimental results of a pristine solid-state nanopore being unable to discriminate between IgG subclasses.[1,2]

In summary, we used graphene nanopores for protein detection using ionic current, dwell time, and water flux

DOI: 10.1021/acs.jpclett.7b00385
J. Phys. Chem. Lett. 2017, 8, 1670−1676

measurements. A total aggregate of 2.7 μs of simulation time was performed for systems with the number of atoms as high as 0.6 million. Each segment of the antibody is shown to be distinguishable by ionic current provided that enough translocation events are available. Using ML and *k*-means clustering, the ionic current−dwell time and water flux−ionic current feature plots generate clusters with far apart centroids. The comparison of a single-atom thick graphene nanopore with a solid-state nanopore (Si_3N_4) reveals that IgG subclasses can not be discriminated with such thick nanopores. A combination of these signals (ionic current and water flux) can greatly contribute to high-precision detection and discrimination between IgGs.

■ ASSOCIATED CONTENT

Supporting Information

The Supporting Information is available free of charge on the ACS Publications website at DOI: 10.1021/acs.jpclett.7b00385.

Different orientations of IgG antibodies in the simulations, conductance calculations, comparison of the conformational changes of IgG2 and IgG3 during translocation, the history of IgG2 translocation through graphene nanopores, and the silicon nitride nanopore simulation setup (PDF)

■ AUTHOR INFORMATION

Corresponding Author

*E-mail: aluru@illinois.edu.

ORCID

Amir Barati Farimani: 0000-0002-2952-8576

Mohammad Heiranian: 0000-0002-2227-4948

Notes

The authors declare no competing financial interest.

■ ACKNOWLEDGMENTS

We thank Professor Emad Tajkhorshid for useful discussions on the protein structures. This work is supported by AFOSR under Grant No. FA9550-12-1-0464 and NSF under Grants 1264282, 1420882, 1506619, and 1545907. We acknowledge the use of the parallel computing resource Blue Waters provided by the University of Illinois and the National Center for Supercomputing Applications.

■ REFERENCES

(1) Wei, R. S.; Gatterdam, V.; Wieneke, R.; Tampe, R.; Rant, U. Stochastic Sensing of Proteins with Receptor-Modified Solid-State Nanopores. *Nat. Nanotechnol.* **2012**, *7*, 257−263.

(2) Yusko, E. C.; Johnson, J. M.; Majd, S.; Prangkio, P.; Rollings, R. C.; Li, J. L.; Yang, J.; Mayer, M. Controlling Protein Translocation through Nanopores with Bio-Inspired Fluid Walls. *Nat. Nanotechnol.* **2011**, *6*, 253−260.

(3) Han, A.; Creus, M.; Schurmann, G.; Linder, V.; Ward, T. R.; de Rooij, N. F.; Staufer, U. Label-Free Detection of Single Protein Molecules and Protein-Protein Interactions Using Synthetic Nanopores. *Anal. Chem.* **2008**, *80*, 4651−4658.

(4) Han, A. P.; Schurmann, G.; Mondin, G.; Bitterli, R. A.; Hegelbach, N. G.; de Rooij, N. F.; Staufer, U. Sensing Protein Molecules Using Nanofabricated Pores. *Appl. Phys. Lett.* **2006**, *88*, 093901.

(5) Kowalczyk, S. W.; Kapinos, L.; Blosser, T. R.; Magalhaes, T.; van Nies, P.; Lim, R. Y. H.; Dekker, C. Single-Molecule Transport across an Individual Biomimetic Nuclear Pore Complex. *Nat. Nanotechnol.* **2011**, *6*, 433−438.

(6) Aksimentiev, A.; Heng, J. B.; Timp, G.; Schulten, K. Microscopic Kinetics of DNA Translocation through Synthetic Nanopores. *Biophys. J.* **2004**, *87*, 2086−2097.

(7) Dekker, C. Solid-State Nanopores. *Nat. Nanotechnol.* **2007**, *2*, 209−215.

(8) Li, J. L.; Gershow, M.; Stein, D.; Brandin, E.; Golovchenko, J. A. DNA Molecules and Configurations in a Solid-State Nanopore Microscope. *Nat. Mater.* **2003**, *2*, 611−615.

(9) Howorka, S.; Cheley, S.; Bayley, H. Sequence-Specific Detection of Individual DNA Strands Using Engineered Nanopores. *Nat. Biotechnol.* **2001**, *19*, 636−639.

(10) Venkatesan, B. M.; Bashir, R. Nanopore Sensors for Nucleic Acid Analysis. *Nat. Nanotechnol.* **2011**, *6*, 615−624.

(11) Farimani, A. B.; Heiranian, M.; Aluru, N. R. Electromechanical Signatures for DNA Sequencing through a Mechanosensitive Nanopore. *J. Phys. Chem. Lett.* **2015**, *6*, 650−657.

(12) Branton, D.; Deamer, D. W.; Marziali, A.; Bayley, H.; Benner, S. A.; Butler, T.; Di Ventra, M.; Garaj, S.; Hibbs, A.; Huang, X. H.; et al. The Potential and Challenges of Nanopore Sequencing. *Nat. Biotechnol.* **2008**, *26*, 1146−1153.

(13) Majd, S.; Yusko, E. C.; Billeh, Y. N.; Macrae, M. X.; Yang, J.; Mayer, M. Applications of Biological Pores in Nanomedicine, Sensing, and Nanoelectronics. *Curr. Opin. Biotechnol.* **2010**, *21*, 439−476.

(14) Steinbock, L. J.; Krishnan, S.; Bulushev, R. D.; Borgeaud, S.; Blokesch, M.; Feletti, L.; Radenovic, A. Probing the Size of Proteins with Glass Nanopores. *Nanoscale* **2014**, *6*, 14380−14387.

(15) Kennedy, E.; Dong, Z. X.; Tennant, C.; Timp, G. Reading the Primary Structure of a Protein with 0.07 nm Resolution Using a Subnanometre-Diameter Pore. *Nat. Nanotechnol.* **2016**, *11*, 968−976.

(16) Derrington, I. M.; Butler, T. Z.; Collins, M. D.; Manrao, E.; Pavlenok, M.; Niederweis, M.; Gundlach, J. H. Nanopore DNA Sequencing with Mspa. *Proc. Natl. Acad. Sci. U. S. A.* **2010**, *107*, 16060−16065.

(17) Purnell, R. F.; Schmidt, J. J. Discrimination of Single Base Substitutions in a DNA Strand Immobilized in a Biological Nanopore. *ACS Nano* **2009**, *3*, 2533−2538.

(18) Deamer, D. W.; Akeson, M. Nanopores and Nucleic Acids: Prospects for Ultrarapid Sequencing. *Trends Biotechnol.* **2000**, *18*, 147−151.

(19) Bayley, H.; Cremer, P. S. Stochastic Sensors Inspired by Biology. *Nature* **2001**, *413*, 226−230.

(20) Plesa, C.; Ruitenberg, J. W.; Witteveen, M. J.; Dekker, C. Detection of Individual Proteins Bound Along DNA Using Solid-State Nanopores. *Nano Lett.* **2015**, *15*, 3153−3158.

(21) Larkin, J.; Henley, R. Y.; Muthukumar, M.; Rosenstein, J. K.; Wanunu, M. High-Bandwidth Protein Analysis Using Solid-State Nanopores. *Biophys. J.* **2014**, *106*, 696−704.

(22) Kong, J. L.; Bell, N. A. W.; Keyser, U. F. Quantifying Nanomolar Protein Concentrations Using Designed DNA Carriers and Solid-State Nanopores. *Nano Lett.* **2016**, *16*, 3557−3562.

(23) Goyal, G.; Lee, Y. B.; Darvish, A.; Ahn, C. W.; Kim, M. J. Hydrophilic and Size-Controlled Graphene Nanopores for Protein Detection. *Nanotechnology* **2016**, *27*, 495301.

(24) Geim, A. K.; Novoselov, K. S. The Rise of Graphene. *Nat. Mater.* **2007**, *6*, 183−191.

(25) Garaj, S.; Hubbard, W.; Reina, A.; Kong, J.; Branton, D.; Golovchenko, J. A. Graphene as a Subnanometre Trans-Electrode Membrane. *Nature* **2010**, *467*, 190−193.

(26) Barati Farimani, A.; Dibaeinia, P.; Aluru, N. R. DNA Origami-Graphene Hybrid Nanopore for DNA Detection. *ACS Appl. Mater. Interfaces* **2017**, *9*, 92−100.

(27) Merchant, C. A.; Healy, K.; Wanunu, M.; Ray, V.; Peterman, N.; Bartel, J.; Fischbein, M. D.; Venta, K.; Luo, Z. T.; Johnson, A. T. C.; Drndic, M. DNA Translocation through Graphene Nanopores. *Nano Lett.* **2010**, *10*, 2915−2921.

(28) Schneider, G. F.; Kowalczyk, S. W.; Calado, V. E.; Pandraud, G.; Zandbergen, H. W.; Vandersypen, L. M. K.; Dekker, C. DNA Translocation through Graphene Nanopores. *Nano Lett.* **2010**, *10*, 3163−3167.

DOI: 10.1021/acs.jpclett.7b00385
J. Phys. Chem. Lett. 2017, 8, 1670−1676

(29) Nelson, T.; Zhang, B.; Prezhdo, O. V. Detection of Nucleic Acids with Graphene Nanopores: Ab Initio Characterization of a Novel Sequencing Device. *Nano Lett.* **2010**, *10*, 3237−3242.
(30) Traversi, F.; Raillon, C.; Benameur, S. M.; Liu, K.; Khlybov, S.; Tosun, M.; Krasnozhon, D.; Kis, A.; Radenovic, A. Detecting the Translocation of DNA through a Nanopore Using Graphene Nanoribbons. *Nat. Nanotechnol.* **2013**, *8*, 939−945.
(31) Sint, K.; Wang, B.; Kral, P. Selective Ion Passage through Functionalized Graphene Nanopores. *J. Am. Chem. Soc.* **2008**, *130*, 16448−16449.
(32) Venkatesan, B. M.; Estrada, D.; Banerjee, S.; Jin, X. Z.; Dorgan, V. E.; Bae, M. H.; Aluru, N. R.; Pop, E.; Bashir, R. Stacked Graphene-Al2o3 Nanopore Sensors for Sensitive Detection of DNA and DNA-Protein Complexes. *ACS Nano* **2012**, *6*, 441−450.
(33) Wells, D. B.; Belkin, M.; Comer, J.; Aksimentiev, A. Assessing Graphene Nanopores for Sequencing DNA. *Nano Lett.* **2012**, *12*, 4117−4123.
(34) Garaj, S.; Liu, S.; Golovchenko, J. A.; Branton, D. Molecule-Hugging Graphene Nanopores. *Proc. Natl. Acad. Sci. U. S. A.* **2013**, *110*, 12192−12196.
(35) Farimani, A. B.; Min, K.; Aluru, N. R. DNA Base Detection Using a Single-Layer Mos2. *ACS Nano* **2014**, *8*, 7914−7922.
(36) Saha, K. K.; Drndic, M.; Nikolic, B. K. DNA Base-Specific Modulation of Microampere Transverse Edge Currents through a Metallic Graphene Nanoribbon with a Nanopore. *Nano Lett.* **2012**, *12*, 50−55.
(37) Zhao, Y.; Zhang, P.; Liu, H.; Sen, S.; Song, W.; Im, J.; Gyarfas, B.; Manna, S.; Biswas, S.; Borges, C.; Lindsay, S.; Ashcroft, B. Single-Molecule Spectroscopy of Amino Acids and Peptides by Recognition Tunnelling. *Nat. Nanotechnol.* **2014**, *9*, 466−473.
(38) Prasongkit, J.; Grigoriev, A.; Pathak, B.; Ahuja, R.; Scheicher, R. H. Transverse Conductance of DNA Nucleotides in a Graphene Nanogap from First Principles. *Nano Lett.* **2011**, *11*, 1941−1945.
(39) Tsutsui, M.; Taniguchi, M.; Yokota, K.; Kawai, T. Identifying Single Nucleotides by Tunnelling Current. *Nat. Nanotechnol.* **2010**, *5*, 286−290.
(40) Taussig, M. J. Studies on Antigenic Competition. 1. Antigenic Competition between Fc and Fab Fragments of Rabbit Igg in Mice. *Immunology* **1971**, *21*, 51.
(41) Kale, L.; Skeel, R.; Bhandarkar, M.; Brunner, R.; Gursoy, A.; Krawetz, N.; Phillips, J.; Shinozaki, A.; Varadarajan, K.; Schulten, K. Namd2: Greater Scalability for Parallel Molecular Dynamics. *J. Comput. Phys.* **1999**, *151*, 283−312.
(42) Guss, B.; Eliasson, M.; Olsson, A.; Uhlen, M.; Frej, A. K.; Jornvall, H.; Flock, J. I.; Lindberg, M. Structure of the Igg-Binding Regions of Streptococcal Protein-G. *EMBO J.* **1986**, *5*, 1567−1575.
(43) Ravetch, J. V.; Kinet, J. P. Fc-Receptors. *Annu. Rev. Immunol.* **1991**, *9*, 457−492.
(44) Harris, L. J.; Larson, S. B.; Hasel, K. W.; McPherson, A. Refined Structure of an Intact Igg2a Monoclonal Antibody. *Biochemistry* **1997**, *36*, 1581−1597.
(45) Michaelsen, T. E.; Frangione, B.; Franklin, E. C. Primary Structure of Hinge Region of Human Igg3 - Probable Quadruplication of a 15-Amino Acid Residue Basic Unit. *J. Biol. Chem.* **1977**, *252*, 883−889.
(46) MacKerell, A. D.; Banavali, N. K. All-Atom Empirical Force Field for Nucleic Acids: Ii. Application to Molecular Dynamics Simulations of DNA and Rna in Solution. *J. Comput. Chem.* **2000**, *21*, 105−120.
(47) Essmann, U.; Perera, L.; Berkowitz, M. L.; Darden, T.; Lee, H.; Pedersen, L. G. A Smooth Particle Mesh Ewald Method. *J. Chem. Phys.* **1995**, *103*, 8577−8593.
(48) Suk, M. E.; Aluru, N. R. Water Transport through Ultrathin Graphene. *J. Phys. Chem. Lett.* **2010**, *1*, 1590−1594.
(49) Lloyd, S. P. Least-Squares Quantization in Pcm. *IEEE Trans. Inf. Theory* **1982**, *28*, 129−137.
(50) Wanunu, M.; Dadosh, T.; Ray, V.; Jin, J. M.; McReynolds, L.; Drndic, M. Rapid Electronic Detection of Probe-Specific Micrornas Using Thin Nanopore Sensors. *Nat. Nanotechnol.* **2010**, *5*, 807−814.

DOI: 10.1021/acs.jpclett.7b00385
J. Phys. Chem. Lett. 2017, 8, 1670−1676